A Hybrid Learning and Model-Based Optimization for HVAC Systems: A Real World Case Study

Dan Wu⋆, Pallavi Bharadwaj⋆, Qing Gao†, and Marija Ilic⋆

***Abstract*—This paper discusses how to effectively integrate learning and model-based methods to optimize economic costs and operational efficiency of heating, ventilation, and air-conditioning (HVAC) systems. By leveraging learning-based methods, heuristics and manufacturing data of each unit in HVAC systems can be well approximated and integrated into the optimization framework. This paper provides an accurate and flexible modeling of an HVAC system to reach a highly economic and efficient daily operation schedule. To demonstrate the efficacy of proposed method, a real world public infrastructure is considered with detailed models and historical operational data. After combining data-driven models and physical models, the overall optimization problem formulation falls into the category of mixed-integer nonlinear optimization, and is further converted into a smooth nonlinear problem for easy-solving. Numerical results are compared to the existing energy consumption record, showing a substantial saving (50%) from the proposed method.**

***Index Terms*—HVAC, Coefficient of Performance, Optimization, Learning-based method, Model-based method**

I. Introduction

Commercial buildings constitute 40% of the present energy consumption in the United States [1]. In order to reduce the carbon footprint of heating, ventilation, and air-conditioning (HVAC) systems' global energy consumption [2], it is crucial to optimize their operational strategies [3]. However, the energy management of commercial buildings is a challenging task [4]. The energy consumption costs in industrial infrastructure find direct correlation with the HVAC constituting more than half the operational cost [5].

In order to solve this HVAC operation optimization problem for reducing cost, increasing efficiency, and improving user comfort [6], both model-based methods [7]–[10] and data-driven methods [4], [11] have been proposed. A majority of the data-driven methods [4], [11] needs a large training dataset and suffers from computational complexity with marginal reduction in operating energy costs. On the other hand, existing model-based methods usually apply approximations such as the RC network models, constant efficiency, and constant coefficient of performance (COP) [12] to simplify the characteristic of each unit as a gray box. Such simplification substantially loses the time-varying features of HVAC units in different working conditions, ignores physical couplings of multi-thermal process within complex units such as flue gas hot water residual heat gas absorption chillers, and disregards thermal couplings between zones [13].

⋆: Laboratory for Information and Decision Systems, Massachusetts Institute of Technology, Cambridge, MA, danwumit@mit.edu, bpallavi@mit.edu, ilic@mit.edu †: ENNEW DIGITAL TECHNOLOGY CO., LTD., gaoqing.ennew.na@gmail.com

Existing work comparing data-driven and model-based methods can be found in [14]. It shows that model-based methods can outperform data-driven methods in accuracy; while data-driven methods can outperform model-based methods in speed. To take advantage of both methods while avoid their drawbacks, we leverage both learning-based methods and model-based methods by formulating an efficient hybrid optimization framework to improve the energy consumption cost of a real world public infrastructure, given its equipment configurations, limited operation data, and environmental records in a period of time.

When dealing with real industrial systems, we were facing the situation of lacking explicit models and measurements for many commercial components. Therefore, we firstly focused on how to construct reasonable models from the limited data by learning-based methods. Specifically, we separate the flue gas hot water residual heat gas absorption chiller into three sub-chillers, and treated their COPs individually with different polynomial fittings. Such separated models are necessary since each sub-chiller has a different energy input source, which is supplied by other units in the station. Ignoring different causal relationships will render less credible results. However, some existing literature considers the flue gas hot water residual heat gas absorption chiller as an integrated component with a single COP. This simplification substantially reduces the flexibility and possibility of finer control within the unit, yielding sub-optimal scheduling. Then, based on the data-driven models we further optimized the total energy consumption for the given historical period of time, and compared to the true energy consumption recorded in the same period to demonstrate the cost improvement gained from the proposed method.

II. HVAC System Modelling

A. A General Description of the Energy Station

The commercial energy station considered in this paper is installed in a real-world public infrastructure. See Fig. 1 [15]. It is supposed to maintain the indoor temperature, humidity, and concentration of carbon dioxide in particular public zones of the infrastructure. There are totally eight cooling, heating and power units in the energy station:

1) Gas-fired generator $\times 2$, Cummins C1160N5C;
2) Flue gas hot water residual heat gas absorption chiller using Lithium-Bromide salt $\times 2$, Broad BZHE400;
3) Direct-fired gas absorption chiller $\times 1$, Broad BZ400;
4) Centrifugal electric chiller $\times 2$, York (Johnson controls) YKM2MRK25DBG;
5) Gas-fired hot water boiler $\times 1$, Tuff Boiler WNSCQ8000.

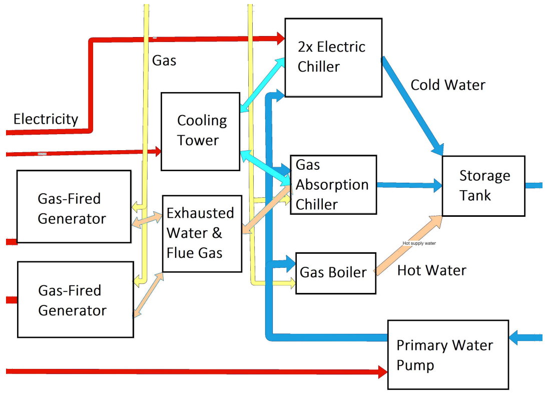

Fig. 1: Energy Station Diagram

According to the energy station record, the direct-fired gas absorption chiller seldom operates (serves as backup unit), and thus, can be safely ignored in our normal optimal operation studies. We focus our investigations on the period from September 1st to September 7th, 2019 with detailed daily temperature and energy consumption data for comparison. From the temperature records it can be implied that cooling was the objective, which further simplifies our model by neglecting the boiler unit.

B. Gas-fired generator

Gas-fired generators are usually fast-ramping units which can reach their rated output power in minutes. In our modeling with the minimum scheduling time interval being 1 hour, we can safely ignore the dynamics of generators and assume they adjust output power in a (quasi) steady state manner. Thus, the generator is modeled as

$$
\begin{aligned}
V_{gg} &= \frac{Q_{gg,rt}\ L_{gg}}{\eta_{gg}\ \gamma_{g2p}} \times 3600\ T && \text{(1a)}\\
\eta_{gg} &= \eta_{gg}(L_{gg}) && \text{(1b)}\\
T_{fg} &= T_{fg}(L_{gg}) && \text{(1c)}\\
M_{fg} &= M_{fg}(L_{gg}) && \text{(1d)}\\
L_{gg,min} &\leq L_{gg} \leq L_{gg,max} && \text{(1e)}
\end{aligned}
$$

where V_{gg} is the gas consumption in m^3; $Q_{gg,rt} = 1160$kW is the rated electric power output [16]; L_{gg} is the unit-less loading level of the generator; $\gamma_{g2p} = 36$ MJ/m^3 is the heat from burning a cubic meter gas [16] (its value can vary according to different compositions of the natural gas); T is the operating hours; η_{gg} is the efficiency of the generator from the input heat power to the output electric power, which is a function of the loading level L_{gg}; T_{fg} is the flue gas temperature in Celsius of the generator, which is a function of the loading level L_{gg}; M_{fg} is the flue gas mass flow rate in kg/s of the generator, which is a function of the loading level L_{gg}; $L_{gg,min} = 0.5$ and $L_{gg,max} = 1.1$ are the minimum and maximum loading levels.

C. Flue gas hot water residual heat gas absorption chiller using Lithium-Bromide salt

The flue gas hot water residual heat gas absorption chiller, abbreviated as “gas absorption chiller”, comprises three different cooling sub-chillers: (1) direct gas-fired sub-chiller, (2) flue gas sub-chiller, and (3) hot water sub-chiller. The direct gas-fired sub-chiller burns natural gas directly to provide cooling (heating). The flue gas sub-chiller uses high temperature flue gas from the gas-fired generator as the power input. The hot water sub-chiller uses the high temperature cooling water out of the gas-fired generator as its input.

Existing literature usually combines these three sub-chillers into one integrated chiller model for simplification. This model blurs their different working characteristics, and loses opportunities of scheduling them separately to achieve a better operating condition. In this paper we treat each sub-chiller individually but also consider their overall interconnected constraints for a more accurate modeling.

1) Direct gas-fired sub-chiller: The direct gas-fired sub-chiller is modeled as follows.

$$
\begin{aligned}
V_{gf} &= \frac{Q_{gf,rt}\ L_{gf}}{\gamma_{g2p}\ \mathrm{COP}_{gf}} \times 3600\ T && \text{(2a)}\\
\mathrm{COP}_{gf} &= \mathrm{COP}_{gf}(L_{gf}, T_{ws}, T_{wc}) && \text{(2b)}\\
L_{gf,min} &\leq L_{gf} \leq L_{gf,max} && \text{(2c)}
\end{aligned}
$$

where V_{gf} is the gas consumption in m^3; $Q_{gf,rt} = 4652$kW is the rated cooling power output [17]; L_{gf} is the unit-less loading level of the gas-fired sub-chiller; COP_{gf} is the COP of gas-fired sub-chiller, which is a function of the loading level L_{gf}, the required supply cold water temperature T_{ws}, and the supply cooling water temperature T_{wc}; $L_{gf,min} = 0.7$ and $L_{gf,max} = 1.15$ are the minimum and maximum loading levels.

2) Flue gas sub-chiller: The flue gas sub-chiller is modeled as follows.

$$
\begin{aligned}
M_{fg} &= \frac{Q_{gf,rt}\ L_{gf}}{\gamma_{fg2p}\ \left(T_{fg} - T_{fg,out}\right)\ \mathrm{COP}_{fg}} && \text{(3a)}\\
\mathrm{COP}_{fg} &= \mathrm{COP}_{fg}(L_{fg}, T_{fg}, T_{ws}, T_{wc}) && \text{(3b)}\\
L_{fg,min} &\leq L_{fg} \leq L_{fg,max} && \text{(3c)}\\
T_{fg,out,min} &\leq T_{fg,out} \leq T_{fg,out,max} && \text{(3d)}
\end{aligned}
$$

where M_{fg} is the input flue gas mass flow rate in kg/s, which is provided by Eqn (1d); T_{fg} is the input flue gas temperature in Celsius, which is provided by Eqn (1c); $T_{fg,out}$ is the output flue gas temperature in Celsius; $\gamma_{fg2p} = 1.2$ kJ/kg °C is the heat capacity of flue gas [17]; $Q_{fg,rt}$ is the rated cooling power output, which can occupy at most 30% of $Q_{gf,rt}$ [17]; L_{fg} is the unit-less loading level of the flue gas sub-chiller; COP_{fg} is the COP of flue gas sub-chiller, which is a function of the loading level L_{fg}, the temperature of the flue gas T_{fg}, the required supply cold water temperature T_{ws}, and the supply cooling water temperature T_{wc}; $L_{fg,min} = 0.6$ and $L_{fg,max} = 1.2$ are the minimum and maximum loading levels; $T_{fg,out,min} = 140$ °C and $T_{fg,out,max} = 300$ °C [17] are minimum and maximum temperatures of the exhausted output flue gas.

3) Hot water sub-chiller: The hot water sub-chiller is modeled as follows.

$$\begin{aligned} M_{hw} &= \frac{Q_{hw,rt}\ L_{hw}}{\gamma_{w2p}\ \big(T_{hw} - T_{hw,out}\big)\ \text{COP}_{hw}} && \text{(4a)}\\ \text{COP}_{hw} &= \text{COP}_{hw}(L_{hw}, T_{hw}, T_{ws}, T_{wc}) && \text{(4b)}\\ L_{hw,min} &\leq\ L_{hw}\ \leq\ L_{hw,max} && \text{(4c)}\\ T_{hw,out,min} &\leq\ T_{hw,out}\ \leq\ T_{hw,out,max} && \text{(4d)} \end{aligned}$$

where $M_{hw} = 19.4$ kg/s is the input hot water mass flow rate [16], which is directly from the generator high temperature cooling water; $T_{hw} = 90$ °C is the input hot water temperature [16], which is the temperature of the generator output cooling water; $T_{hw,out}$ is the hot water output temperature in Celsius; $\gamma_{w2p} = 4.2$ kJ/kg °C is the heat capacity of water [17]; $Q_{hw,rt}$ is the rated cooling power output, which can occupy at most 23% of $Q_{gf,rt}$ [17]; L_{hw} is the unit-less loading level of the hot water sub-chiller; COP$_{hw}$ is the COP of hot water sub-chiller, which is a function of the loading level L_{hw}, the temperature of the hot water T_{hw}, the required supply cold water temperature T_{ws}, and the supply cooling water temperature T_{wc}; $L_{hw,min} = 0.5$ and $L_{hw,max} = 1.1$ are the minimum and maximum loading levels; $T_{hw,out,min}$ and $T_{hw,out,max} = 80$ °C [16] are minimum and maximum temperatures of the exhausted output hot water.

4) Overall interaction constraints on all sub-chillers: As stated above, the gas absorption chiller has three sub-chillers working together to provide the desired cooling (heating) capacity. From the manufacturing specifics in [17], they must satisfy an overall cooling capacity constraint, which is stated below.

$$0.05 \leq s_{gf}L_{gf} + \frac{s_{gg}\Big(Q_{fg,rt}L_{fg} + Q_{hw,rt}L_{hw}\Big)}{Q_{gf,rt}} \leq 1.15 \quad (5)$$

where s_{gf} is the binary variable taking values between 1 and 0 that indicates whether the direct gas-fired sub-chiller is on or off; s_{gg} is the binary variable taking values between 1 and 0 which indicates whether the gas-fired generator is on or off.

D. Centrifugal electric chiller

The centrifugal electric chiller is equipped with variable speed controllers. However, the manufacturing book [18] does not provide detailed COP data in different working conditions. Therefore, we have to make an optimistic assumption that the COP is a constant value whatever the loading level is. The chiller model is given below.

$$\begin{aligned} E_{cc} &= \frac{Q_{cc,rt}\ L_{cc}}{\text{COP}_{cc}} && \text{(6a)}\\ L_{cc,min} &\leq\ L_{cc}\ \leq\ L_{cc,max} && \text{(6b)}\\ & && \text{(6c)} \end{aligned}$$

where $Q_{cc,rt} = 4571$kW is the rated cooling power [18]; L_{cc} is the unit-less loading level of the centrifugal chiller; COP$_{cc} = 5.615$ is the COP of centrifugal electric chiller, which is calculated at the rated power condition; $L_{cc,min} = 0.05$ and $L_{cc,max} = 1.0$ are the assumed minimum and maximum loading levels.

III. Learning Manufacturing Heuristics

Recall Eqn (1b), (1d), (1c), (2b), (3b), and (4b), they capture important unit characteristics under different operating conditions. However, these characteristics are implicitly defined and influenced by many factors, for example, the structural designs of equipments, properties of different materials, and very complicated physical processes. To obtain an accurate heuristic model, we apply the polynomial fitting technique to learn basic characteristic functions for different working conditions.

Specifically, polynomials are used to approximate these characteristics. Since manufacturing tests were carried out for a limited working conditions, we restrict our highest polynomial degree to 2 to avoid over-fitting.

$$\begin{aligned} \eta_{gg} &= a_{\eta_{gg}}L_{gg}^2 + b_{\eta_{gg}}L_{gg} + c_{\eta_{gg}} && \text{(7a)}\\ M_{fg} &= a_{M_{fg}}L_{gg}^2 + b_{M_{fg}}L_{gg} + c_{M_{fg}} && \text{(7b)}\\ T_{fg} &= a_{T_{fg}}L_{gg}^2 + b_{T_{fg}}L_{gg} + c_{T_{fg}} && \text{(7c)}\\ \text{COP}_r &= a_{\text{COP}_r}L_r^2 + b_{\text{COP}_r}L_r + c_{\text{COP}_r} &&\\ &+\ A_{\text{COP}_r}T_r^2 + B_{\text{COP}_r}T_r + C_{\text{COP}_r} &&\\ &+\ u_{\text{COP}_r}T_{ws}^2 + v_{\text{COP}_r}T_{ws} + w_{\text{COP}_r} &&\\ &+\ \alpha_{\text{COP}_r}T_{wc}^2 + \beta_{\text{COP}_r}T_{wc} + \theta_{\text{COP}_r} && \text{(7d)} \end{aligned}$$

where a, A, u, and α are the coefficients for the quadratic terms; b, B, v, and β are the coefficients for the linear terms; and c, C, w, and θ are the coefficients for constant terms; subscript COP means the coefficient associated with COP; both subscript and sub-subscript $r \in \{gf, fg, hw\}$ in which "gf" means gas-fired generator, "fg" means flue gas sub-chiller, and "hw" means hot water sub-chiller. When $r = gf$, the $A_{\text{COP}_{gf}} = B_{\text{COP}_{gf}} = C_{\text{COP}_{gf}} = 0$.

According to [17], in the direct gas-fired sub-chiller once L_{gf} and T_{ws} are given, the cooling water temperature T_{wc} can be uniquely determined by the look-up chart, suggesting a mapping $f : (L_{gf}, T_{ws}) \mapsto T_{wc}$. It is also the case for the flue gas sub-chiller $g : (L_{fg}, T_{fg}, T_{ws}) \mapsto T_{wc}$ and the hot water sub-chiller $h : (L_{hw}, T_{hw}, T_{ws}) \mapsto T_{wc}$. Thus, we can safely drop the terms associated with the cooling water temperature T_{wc} in (7d), yielding

$$\begin{aligned} \text{COP}_r &= a_{\text{COP}_r}L_r^2 + b_{\text{COP}_r}L_r + c_{\text{COP}_r} &&\\ &+\ A_{\text{COP}_r}T_r^2 + B_{\text{COP}_r}T_r + C_{\text{COP}_r} &&\\ &+\ u_{\text{COP}_r}T_{ws}^2 + v_{\text{COP}_r}T_{ws} + w_{\text{COP}_r} && \text{(8)} \end{aligned}$$

Regression techniques are applied to learn the coefficients in (7a), (7b), (7c), and (8). The root mean square error (rmse) of the multi-variable polynomial fitting for each unit is less than 2% in our particular real-world energy station example.

IV. Overall Optimization Formulation

Once the characteristic functions of (1b), (1d), (1c), (2b), (3b), and (4b) have been learned, each unit is well-defined. Hence, we can formulate the overall optimization problem for the daily scheduling.

$$\text{min:} \quad \sum_{k=1}^{K}\sum_{i=1}^{2}\Big(s_{gg,i}[k]\ V_{gg,i}[k]\ C_{gas}[k]$$

$$
\begin{aligned}
& +s_{gf,i}[k]\ V_{gf,i}[k]\ C_{gas}[k] \\
& +s_{cc,i}[k]\ E_{cc,i}[k]\ C_{e,buy}[k] \\
& \left. +s_{gg,i}[k]\ Q_{gg,rt}\ L_{gg,i}[k]\ C_{e,sale}[k]\ T[k] \right) \quad \text{(9a)} \\
\text{s.t.:} \quad & \text{Eqn. (1) (2) (3) (4) (5) (6)} \quad \text{(9b)} \\
& \Big(s_{gg,i}[k]\ L_{fg,i}[k]\ Q_{fg,rt} + \\
& s_{gg,i}[k]\ L_{hw,i}[k]\ Q_{hw,rt} + \\
& s_{gf,i}[k]\ L_{gf,i}[k]\ Q_{gf,rt} + \\
& s_{cc,i}[k]\ L_{cc,i}[k]\ Q_{cc,rt} \Big)\ T[k] \geq Q_{ld}[k] \quad \text{(9c)} \\
& i = \{1, 2\} \quad \text{(9d)} \\
& s_{gg,i}[k],\ s_{gf,i}[k],\ s_{cc,i}[k] = \{0, 1\} \quad \text{(9e)}
\end{aligned}
$$

where k indicates different periods in a day; K means the total number of time periods; subscript i indicates the numbering of the unit; $s_{gg,i}$, $s_{gf,i}$, and $s_{cc,i}$ are binary variables that determine if the associated units are on or off; C_{gas} is the natural gas purchase price RMB/m^3; $C_{e,buy}$ is the electricity purchase price RMB/kWh; $C_{e,sale}$ is the electricity sale price RMB/kWh, which should take the negative value if we regard spending as positive; Q_{ld} is the cooling load demand in kWh.

The objective function (9a) sums up the total gas expenditure, total electricity expenditure, and the total electricity sale revenue. Constraint (9c) indicates that at each time step k the total heat removal should not be less than the minimum cooling $Q_{ld}[k]$, which is the minimum accumulative heat removal to achieve the intra-hourly temperature control.

Problem (9) is a mixed-integer nonlinear optimization problem which is usually hard to solve. We relax the binary constraint (9e) by the following inequalities to make the problem continuous. Once solved by some smooth optimization solver, the relaxed binary variables are rounded to the nearest integers. Then, fixing all the binary variables and re-run the smooth solver to obtain the optimal scheduling under this unit commitment configuration.

$$
s_{t,i}[k]\ (s_{t,i}[k] - 1) \leq 0 \quad (10)
$$

where subscript $t \in \{gg, gf, cc\}$. Hence, the overall unknown variables include $s_{gg,i}[k]$, $L_{gg,i}[k]$, $\eta_{gg,i}[k]$, $T_{fg,i}[k]$, $M_{fg,i}[k]$, $V_{gg,i}[k]$, $s_{gf,i}[k]$, $L_{gf,i}[k]$, $\mathrm{COP}_{gf,i}[k]$, $V_{gf,i}[k]$, $L_{fg,i}[k]$, $Z_{fg,i}[k]$, $T_{fg,out,i}[k]$, $\mathrm{COP}_{fg,i}[k]$, $L_{hw,i}[k]$, $T_{hw,out,i}[k]$, $\mathrm{COP}_{hw,i}[k]$, $s_{cc,i}[k]$, $L_{cc,i}[k]$, and $E_{cc,i}[k]$ for all i and k.

V. Numerical Simulations

Numerical simulations are conducted in Matlab 2017 environment on a 64-bit personal computer with an Intel i7 2.8GHz CPU and 16GB RAM. The primal-dual interior point solver "IPOPT" [19] is used for solving the continuous problem.

Based on the energy station record from Sep 1st to Sep 7th, 2019, our model yields an optimal scheduling for that week. Each day is divided into 8 subsequent periods based on different electricity purchase prices. They are listed in Table I. So $k = 1, \ldots, 8$ in (9a). Each period demand $Q_{ld}[k]$ in (9c) is provided by the record so that our problem formulation forces any feasible solution to satisfy the historical data. Then, we can compare our solved optimal scheduling to the record scheduling, which are presented in Fig. 2 - 5.

Fig. 2 shows that our optimized electricity consumption is generally much lower than the historical record for all periods. Fig. 3 suggests that the energy station should generate more electricity for sale to gain more benefits. Fig. 4 tells that the optimized gas consumption from our model is much higher than the record for all periods. Based on the same cost function formula (9a), we can compare our optimized cost values to the calculated historical cost values based on the electricity and gas consumption record. The results are shown in Fig. 5,

TABLE I: Daily Periods and Unit Prices

Time Period	Purchase Price (RMB/kWh)	Sale Price (RMB/kWh)	Gas Price (RMB/m^3)
00:00 - 07:00	0.3941	0.6633	2.92
07:00 - 08:00	0.5941	0.6633	2.92
08:00 - 11:00	0.7441	0.6633	2.92
11:00 - 15:00	0.5941	0.6633	2.92
15:00 - 19:00	0.7441	0.6633	2.92
19:00 - 22:00	0.8441	0.6633	2.92
22:00 - 23:00	0.5941	0.6633	2.92
23:00 - 00:00	0.3941	0.6633	2.92

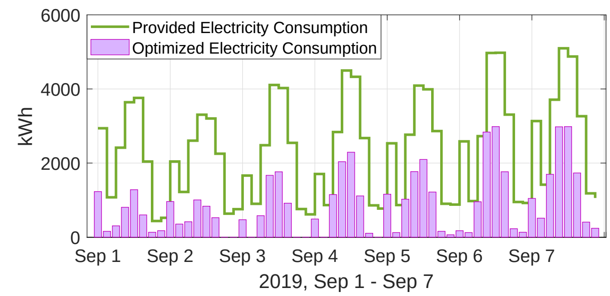

Fig. 2: Electricity Consumption Comparison

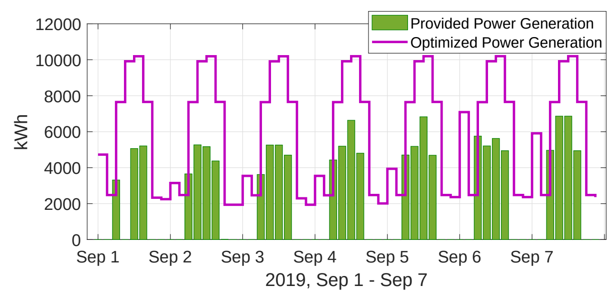

Fig. 3: Electricity Generation Comparison

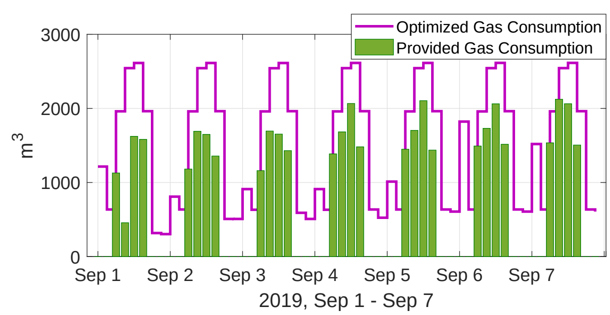

Fig. 4: Gas Consumption Comparison

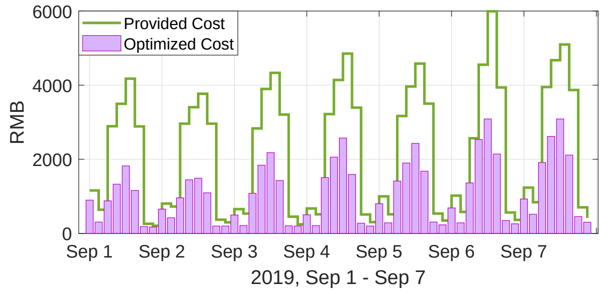

Fig. 5: Cost Comparison

indicating a substantial saving on the total monetary spending. The whole week's spending from our optimized result is $6,1430$ RMB, which only occupies 50.05% of the calculated historical cost value at $122,740$ RMB. This improvement is at least 12% higher than the state of the art methods [5].

Our optimized scheduling results also suggest that two gas-fired generators are always in operation during the whole week, which contributes to the high consumption of the natural gas. Although the gas price is not cheap, the gas-fired generators convert the gas into electricity for sale, and the flue gas and hot water from gas-fired generators are used in the flue gas sub-chiller and the hot- water sub-chiller. So, the entire energy cost turns out to be lower than using electricity. The direct gas-fired sub-chillers remains inactive for the whole week. The centrifugal electric chillers are active only when the flue gas and hot water sub-chillers cannot satisfy the total demand requirement.

VI. Conclusion

In this work we proposed a hybrid learning and model-based optimization framework to minimize the operation cost of HVAC system in a real world commercial energy station. Instead of assuming a gray box for complex multi-thermal process HVAC unit with constant characteristics, we leveraged learning-based methods to acquire accurate and varying heuristic models for internal sub-units and formulated their interaction constraints. Then, an overall model-based optimization framework is proposed and solved to obtain the minimum daily operation cost while satisfying the total cooling demand. When applied to a real world commercial energy station, the proposed hybrid learning and model-based method achieved a substantial saving in energy cost, compared to the historical data. The comparison suggests a reduced energy cost by 50%, provided credible historical data, making it at least 12% more efficient than the state-of-the-art methods. Future work is needed to combine the proposed method with more granular control designs that adjust indoor temperature, humidity, and carbon dioxide density while still optimize the overall energy consumption efficiency.

Acknowledgement

This work is funded by ENN Digital for the project Dynamic Monitoring and Decision Systems (DyMonDS) framework for IT-enabled engineering of retail-level energy services (RES) through MIT Energy Initiative.

References

[1] M. Ostadijafari, A. Dubey, and N. Yu, "Linearized price-responsive hvac controller for optimal scheduling of smart building loads," *IEEE Transactions on Smart Grid*, vol. 11, no. 4, pp. 3131–3145, 2020.

[2] N. Chakraborty, A. Mondal, and S. Mondal, "Multiobjective optimal scheduling framework for hvac devices in energy-efficient buildings," *IEEE Systems Journal*, vol. 13, no. 4, pp. 4398–4409, 2019.

[3] X. Guan, Z. Xu, and Q. Jia, "Energy efficient buildings facilitated by micro grid," in *IEEE PES General Meeting*, pp. 1–1, 2010.

[4] A. Jindal, N. Kumar, and J. J. P. C. Rodrigues, "A heuristic-based smart hvac energy management scheme for university buildings," *IEEE Transactions on Industrial Informatics*, vol. 14, no. 11, pp. 5074–5086, 2018.

[5] K. H. Khan, C. Ryan, and E. Abebe, "Day ahead scheduling to optimize industrial hvac energy cost based on peak/off-peak tariff and weather forecasting," *IEEE Access*, vol. 5, pp. 21684–21693, 2017.

[6] B. Liu, M. Akcakaya, and T. E. Mcdermott, "Automated control of transactive hvacs in energy distribution systems," *IEEE Transactions on Smart Grid*, vol. 12, no. 3, pp. 2462–2471, 2021.

[7] M. Vasak, A. Banjac, N. Hure, H. Novak, D. Marusic, and V. Lesic, "Modular hierarchical model predictive control for coordinated and holistic energy management of buildings," *IEEE Transactions on Energy Conversion*, pp. 1–1, 2021.

[8] K. Ojand and H. Dagdougui, "Q-learning-based model predictive control for energy management in residential aggregator," *IEEE Transactions on Automation Science and Engineering*, pp. 1–12, 2021.

[9] D. T. Vedullapalli, R. Hadidi, and B. Schroeder, "Combined hvac and battery scheduling for demand response in a building," *IEEE Transactions on Industry Applications*, vol. 55, no. 6, pp. 7008–7014, 2019.

[10] P. Bharadwaj, J. Agrawal, R. Jaddivada, M. Zhang, and M. Ilic, "Measurement-based validation of energy-space modelling in multi-energy systems," in *2020 52nd North American Power Symposium (NAPS)*, pp. 1–6, IEEE, 2021.

[11] Y.-E. Jang, Y.-J. Kim, and J. P. S. Catalo, "Optimal hvac system operation using online learning of interconnected neural networks," *IEEE Transactions on Smart Grid*, vol. 12, no. 4, pp. 3030–3042, 2021.

[12] H. Shi, J. Liu, and Q. Chen, "An rc-network approach for hvac precooling optimization in buildings," *IEEE Transactions on Sustainable Computing*, pp. 1–1, 2019.

[13] Y. Yang, G. Hu, and C. J. Spanos, "Hvac energy cost optimization for a multizone building via a decentralized approach," *IEEE Transactions on Automation Science and Engineering*, vol. 17, no. 4, pp. 1950–1960, 2020.

[14] X. Kou, Y. Du, F. Li, H. Pulgar-Painemal, H. Zandi, J. Dong, and M. M. Olama, "Model-based and data-driven hvac control strategies for residential demand response," *IEEE Open Access Journal of Power and Energy*, vol. 8, pp. 186–197, 2021.

[15] D. Wu, J. Agrawal, P. Bharadwaj, L. Li, J. Zhang, and M. Ilic, "On the validity of decomposition for distributed parameter estimation in complex dynamical systems: The case of cooling systems," in *2020 52nd North American Power Symposium (NAPS)*, pp. 1–6, 2021.

[16] Cummins Inc., "Generator set data sheet 1160kw continuous." https://www.cummins.com/sites/default/files/2020-02/C1160N5C\%20-d-3239.pdf, 2021. [Online; accessed 8-Nov-2021].

[17] Broad Group, "Broad xi non-electric chiller model selection & design manual." https://www.broadusa.net/en/wp-content/uploads/2015/03/BROAD-XI-NON-ELECTRIC-CHILLER.pdf, 2021. [Online; accessed 8-Nov-2021].

[18] Johnson Controls, "Model yk style h centrifugal liquid chillers." https://docs.johnsoncontrols.com/chillers/api/khub/documents/jMPftZuK2wWVXODkAKqRSQ/content, 2021. [Online; accessed 8-Nov-2021].

[19] A. Wächter and L. T. Biegler, "On the implementation of an interior-point filter line-search algorithm for large-scale nonlinear programming," *Mathematical programming*, vol. 106, no. 1, pp. 25–57, 2006.